

Research Paper

Statistical study of EMIC Pc1–Pc2 waves observed at subauroral latitudes



Jong-Woo Kwon^a, Khan-Hyuk Kim^{a,*}, Ho Jin^a, Hyuck-Jin Kwon^a, Geonhwa Jee^{b,c}, Kazuo Shiokawa^d, Martin Connors^e

^a School of Space Research, Kyung Hee University, Gyeonggi, South Korea

^b Division of Climate Change Research, Korea Polar Research Institute, Incheon, South Korea

^c Department of Polar Science, Korea University of Science and Technology, Daejeon, South Korea

^d Institute for Space–Earth Environmental Research, Nagoya University, Nagoya, Japan

^e Centre for Science, Athabasca University, Athabasca, Alberta, Canada

ARTICLE INFO

Keywords:

Pc1–Pc2 waves
Subauroral latitude
He-band
Plasmapause

ABSTRACT

Although the occurrence rate of electromagnetic ion cyclotron (EMIC) waves is high in the outer magnetosphere ($L > 7$), it has been suggested in the past that a steep plasma density gradient region of the plasmapause is a preferred location for the generation of EMIC waves. To examine spectral properties of the EMIC waves occurred near the nominal location of the plasmapause ($L = 4–5$), we focus on Pc1–Pc2 waves observed at subauroral latitude Athabasca station (magnetic latitude: $\sim 62^\circ$, and $L \sim 4.6$). A statistical study of 10,494 wave samples identified from Athabasca data for 2007–2008 reveals the following wave characteristics. (1) Wave frequencies are higher in the postmidnight-to-dawn sector and lower in the late afternoon sector. (2) They mostly appear to be in frequency band between helium and oxygen gyrofrequencies (i.e., He-band) calculated from the dipole field model magnetic field intensity at $L = 4.6$. (3) The occurrence rate of Pc1–Pc2 waves has a peak in the prenoon sector at 0900–1100 LT under quiet geomagnetic conditions ($Kp \leq 1$), but is peaked in the afternoon sector under moderate and disturbed geomagnetic conditions ($Kp \geq 2$). (4) The Pc1–Pc2 waves observed at Athabasca were composed of a mixture of left-hand, right-hand, and linearly polarized waves. By comparing previous and recent studies with these observations, we suggest that the subauroral latitude Pc1–Pc2 waves are associated with EMIC waves generated near the plasmapause and discuss the EMIC wave properties in a region of cold and dense plasmas containing heavy ions in the inner magnetosphere.

1. Introduction

Ultra-low frequency (ULF) waves in the Pc1–Pc2 band (0.1–5 Hz) are extensively observed on the ground at low to high latitudes (e.g., Engebretson et al., 2002; Bortnik et al., 2008; Nomura et al., 2011; Mann et al., 2014; Kim et al., 2016a) and are considered to be generated by the electromagnetic ion cyclotron (EMIC) instability near the magnetospheric equatorial region over a wide range of L ($\sim 4–12$) (e.g., Anderson et al., 1992a, 1992b; Fraser and Nguyen, 2001; Min et al., 2012; Usanova et al., 2012; Keika et al., 2013; Saikin et al., 2015; Kim et al., 2016c). The EMIC instability requires a thermal anisotropic distribution of the hot ions (Cornwall, 1965; Kennel and Petschek, 1966). The thermal anisotropy for EMIC wave generation occurs as energetic ($\sim 10–100$ keV) ions are injected into the inner magnetosphere from the magnetotail by enhanced Earthward convection during storm and sub-storm intervals (e.g., Ishida et al., 1987; Erlandson and Ukhorskiy, 2001;

Jordanova et al., 2008), and is also caused by external variations in the solar wind dynamic pressure (e.g., Olson and Lee, 1983; Engebretson et al., 2002, 2015; Usanova et al., 2008; Kim et al., 2017).

It has been known that the heavy ions (He^+ and O^+) in the magnetospheric plasma play a significant role in determining the spectral and propagation properties of EMIC waves by introducing additional cutoff, resonance, crossover, and bi-ion frequencies (Young et al., 1981; Mauk et al., 1981; Roux et al., 1982; Kozyra et al., 1984). In the presence of He^+ and O^+ , the wave's dispersion relation is split into three branches, and the relative growth of EMIC waves in the branches depends on the density of the heavy ions. For example, if the density of He^+ in the cold plasma increases, then the wave growth is enhanced below the He^+ gyrofrequency (i.e., in the He-band between the He^+ gyrofrequency and O^+ gyrofrequency), while it is reduced above the He^+ gyrofrequency (i.e., in the H-band between the H^+ gyrofrequency and He^+ gyrofrequency) (e.g., Kozyra et al., 1984).

* Corresponding author.

E-mail address: khan@khu.ac.kr (K.-H. Kim).

<https://doi.org/10.1016/j.jastp.2020.105292>

Received 13 August 2019; Received in revised form 13 January 2020; Accepted 27 April 2020

Available online 11 May 2020

1364-6826/© 2020 Elsevier Ltd. All rights reserved.

THEMIS spacecraft observations of EMIC waves over $L = 6$ – 12 show that the maximum occurrence rate of H-band waves appears in the early morning sector at $L = 10$ – 12 in the lower cold density region and that the He-band EMIC waves are mainly localized between 1200 and 1800 magnetic local time (MLT) at $L = 7$ – 10 in the higher cold density region (Min et al., 2012; Kim et al., 2016c). One outstanding feature of He-band EMIC waves observed at THEMIS is that the high He-band occurrence appears at a steep density gradient region (Kim et al., 2016c). Although such a region is located more outward than a typical plasmopause ($L \sim 4$ – 5), it was identified with the plasmopause by Kwon et al. (2015), who reported that the plasmopause is located above geosynchronous orbit under quiet geomagnetic conditions and confirmed a plasmaspheric bulge in the late afternoon sector under moderate geomagnetic conditions. Thus, THEMIS observations suggest that the source of He-band waves is near or at the gradient in the cold plasmaspheric density associated with the plasmopause. The He-band waves observed at geosynchronous orbit exhibit a peak occurrence near noon (1100–1200 MLT) under quiet geomagnetic conditions and around the afternoon sector (1500–1600 MLT) for all geomagnetic conditions (Park et al., 2016). This local time dependence of the geosynchronous He-band wave occurrence on geomagnetic conditions is also interpreted as a radial cold plasma density distribution along the local time near geosynchronous orbit.

Previous studies on EMIC waves using spacecraft data obtained in the inner magnetosphere ($L < 7$) reported that EMIC waves are not associated with large local density gradient (i.e., plasmopause) even though the wave's occurrence is high in regions of enhanced cold densities (e.g., Fraser and Nguyen, 2001; Halford et al., 2015). Recently, Tetrick et al. (2017) examined the spatial location of EMIC waves observed in the inner magnetosphere relative to the plasmopause and reported that most of EMIC waves occurred over an L range from -1 to $+2 R_E$ relative to the plasmopause location. They also reported that He-band EMIC waves dominated in all local time sectors inside the plasmopause and at the plasmopause. However, H-band waves are not observed inside the plasmopause.

The objective of the present study is to provide the spectral properties of subauroral latitude Pc1-Pc2 waves observed at Athabasca station ($L \sim 4.6$) during the period of 2007–2008. This study is motivated by a recent case study of long-lasting (>20 h) EMIC Pc1-Pc2 waves observed at Athabasca ($L \sim 4.6$) and CARISMA stations ($L \sim 4$ – 6) on April 5, 2007 (Kim et al., 2016a). The authors reported that the frequencies of the long-lasting waves are in the He-band and depend on local time (i.e., the minimum frequency near dusk and the maximum frequency near dawn). The local time dependent frequency signature is localized in a region of $L = 4$ – 6 . Mann et al. (2014) presented a case of long duration (>18 h) EMIC Pc1-Pc2 waves observed at CARISMA stations. The long-lasting wave's frequency also depends on local time and such a frequency-dependent structure is localized within $L < 6$.

In the present study, we statistically examine whether the wave signatures reported by Kim et al. (2016a) and Mann et al. (2014) are typical spectral properties of subauroral latitude Pc1-Pc2 waves and also examine whether there is a local time dependence of subauroral Pc1-Pc2 wave occurrence on geomagnetic conditions. We show that Pc1-Pc2 waves at subauroral latitudes mostly appear in the He-band and their frequencies are local time dependent, which is similar to the observations of the previous case studies. We suggest that the subauroral latitude Pc1-Pc2 waves are associated with EMIC waves generated near the plasmopause.

The remainder of the paper is organized as follows. Section 2 presents the data set for this study. Section 3 describes the examples of subauroral latitude Pc1-Pc2 waves. Section 4 presents statistical analyses of the Pc1-Pc2 waves. Section 5 presents discussion, and section 6 concludes the study.

2. Data set

The magnetic field data from the induction magnetometer (Shiokawa et al., 2010) at Athabasca in Canada were used to detect subauroral latitude Pc1-Pc2 pulsations for a 2-year period from January 2007 to December 2008. Athabasca is located at a geographic longitude of 246.7° E and geographic latitude of 54.7° N on a magnetic L shell of ~ 4.6 (magnetic latitude of $\sim 62^\circ$) according to the Altitude Adjusted Corrected Geomagnetic (AACGM) system (Shepherd, 2014). The induction magnetometer measures magnetic field variations with a sampling rate of 64 Hz. We also used magnetic fields measured from the fluxgate magnetometer onboard the GOES 11 satellite (Singer et al., 1996) at geosynchronous orbit ($L \sim 6.7$) to examine whether the wave activities seen at Athabasca are spatially localized within geosynchronous orbit. GOES 11 was located at geographic longitude of 225° E, 1.5 h west of the Athabasca station. The original time resolution of the GOES fluxgate magnetic field data used for this study is 0.512 s, and we resampled the GOES data to 0.6 s. Fig. 1 shows the location of the Athabasca ground station and the magnetic conjugation of GOES 11 satellite to the ground. The satellite conjugation was calculated using the magnetic field model of T98c (Tsyganenko, 1989) for $Kp = 2$. The dashed curves on the map indicate the corrected geomagnetic latitudes at 67.3° and 62.2° , calculated from the IGRF model. The L values corresponding to the geomagnetic latitudes are also shown in Fig. 1.

3. Examples of Pc1-Pc2 waves at subauroral latitude

Figs. 2a–c show the dynamic power spectra of the transverse b_x component at GOES 11 and the horizontal H (northward) and D (eastward) components at the Athabasca station for the interval of 09:00–24:00 universal time (UT) on March 10, 2007. The geomagnetic activity was quiet ($Kp \leq 1$) during the 12-h interval of the 09:00–24:00 UT interval as the 3-h Kp values are displayed on the top of Fig. 2a. The local times of GOES 11 (G11LT) and Athabasca station (ATHLT) are shown at the bottom. Two white lines in Fig. 2a indicate the local helium (f_{He+}) and oxygen (f_{O+}) gyrofrequencies at geosynchronous orbit. The gyrofrequencies plotted in Fig. 2b and c are the estimated values at the equatorial plane for the Athabasca L shell ($L = 4.6$) by using the dipole field model.

There is no wave activity above f_{He+} and between f_{He+} and f_{O+} in the GOES 11 dynamic spectra for 15-h interval while GOES 11 moved from midnight to afternoon. However, time-modulated wave activities are clearly seen in the dynamic power spectra of the H and D components of Athabasca station, located with a small local time separation (1.5 h)

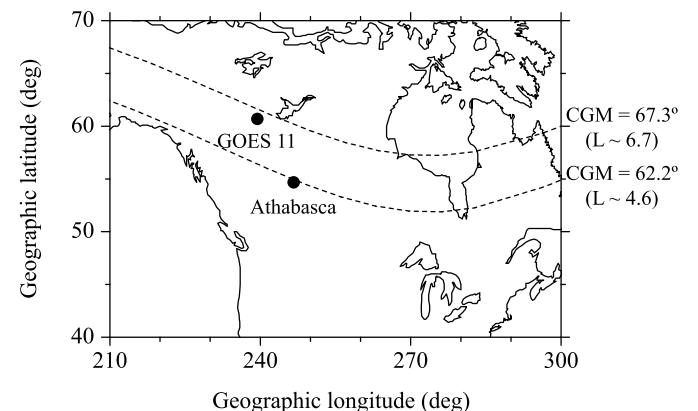


Fig. 1. The location of the Athabasca ground station and the magnetic conjugation of GOES 11 satellite to the ground. The dashed curves on the map indicate corrected geomagnetic latitudes at 67.3° and 62.2° , calculated from the IGRF model. The L values corresponding to the geomagnetic latitudes are shown to the right.

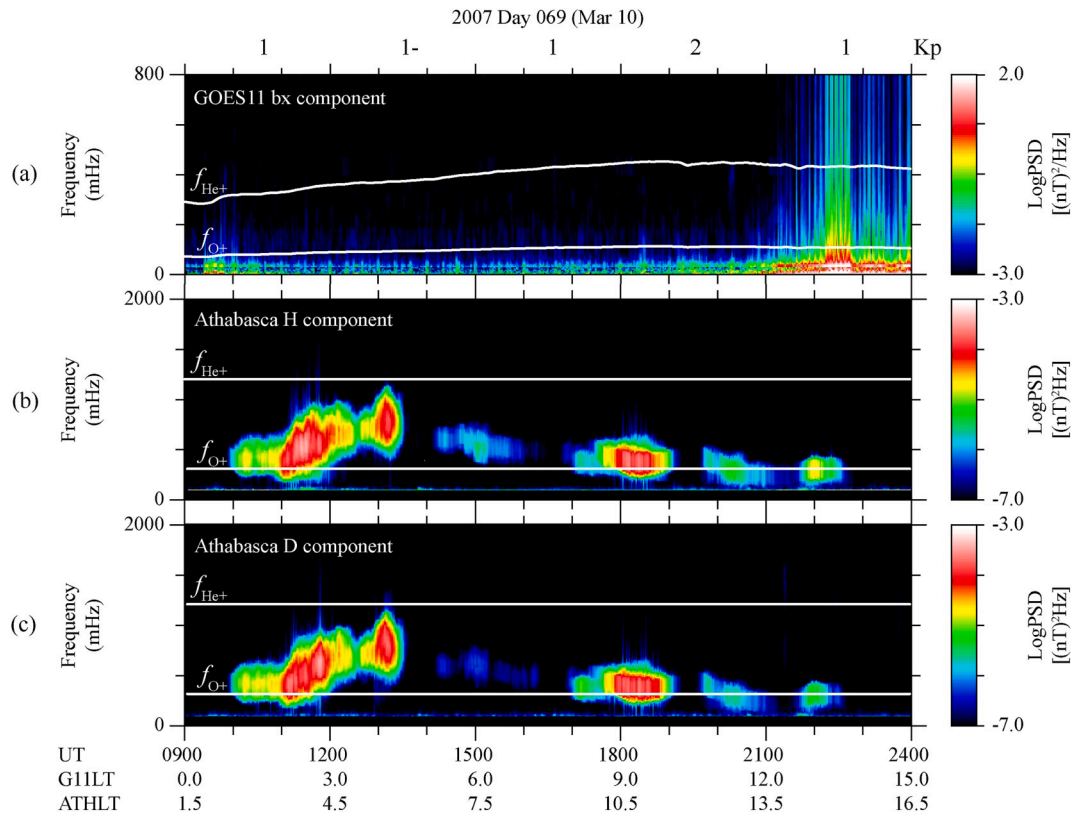


Fig. 2. The dynamic power spectra of (a) the transverse b_x component at GOES 11, and (b) the horizontal H (northward) and (c) D (eastward) components at the Athabasca station for the interval of 09:00–24:00 universal time (UT) on March 10, 2007. Two white lines in Fig. 2a indicate the local helium (f_{He^+}) and oxygen (f_{O^+}) gyrofrequencies at geosynchronous orbit. The gyrofrequencies plotted in Fig. 2b and Fig. 2c are the estimated values at the equatorial plane for the Athabasca L shell ($L = 4.6$) by using the dipole field model.

from GOES 11, for several hours. The spectra show a band structure in the Pc1-Pc2 frequency range and are mostly enhanced between f_{He^+} and f_{O^+} . These observations indicate that the Pc1-Pc2 waves at Athabasca are radially localized inside geosynchronous orbit. One outstanding feature to be noted in the dynamic spectra is the local time (LT) dependence of the frequency in the Pc1-Pc2 band (0.1–5 Hz). The frequency increases for the interval of 10:00–13:30 UT while the Athabasca station moved from postmidnight (~ 2.5 LT) to dawn (~ 6.0 LT), and then falls monotonically to 22:00 UT (~ 14.5 LT) with LT. This LT dependence is very similar to that of long-lasting Pc1-Pc2 waves reported by Kim et al. (2016a).

Fig. 3 shows the spectral analysis of the horizontal H and D components of the Athabasca data for a 3 min interval (12:00–12:03 UT) selected from the data shown in Fig. 2. Fig. 3a demonstrates the power spectral density for the Athabasca H and D components (PSD H and PSD D) and total horizontal power density defined to be PSD $H + \text{PSD } D$. The spectral peak of the total PSD is in the Pc1 frequency range of 0.2–5 Hz and marked by a solid circle. In Fig. 3b, the coherence (γ) defined according to Bendat and Piersol (2010) and the degree of polarization (R) described by Fowler et al. (1967) are computed for the Athabasca H and D data. If γ (R) is greater than 0.7 (0.8), it is called a high-coherence (high degree of polarization) event in this study. The ellipticity in Fig. 3c is defined to be negative if the sense of rotation is in the direction of ion gyromotion (i.e., left-handed polarization) and positive if it is in the direction of electron gyromotion (i.e., right-handed polarization). If the ellipticity is 0 or ± 1 , the wave is linearly or circularly polarized. At the peak of the total PSD shown in Fig. 3, the coherence and degree of the polarization are ~ 0.8 and ~ 0.9 , respectively, and the Pc1 wave is left-handed polarized.

Fig. 4 shows the spectral parameters of the wave samples extracted from the Athabasca H and D data for the interval shown in Fig. 2. To

identify each wave sample, the spectral analysis used in Fig. 3 was done continuously in non-overlapping 3-min segments of the time series. Fig. 4a shows peak frequency (f_{peak}) of wave samples, which reproduces a major feature, i.e., the local time dependence of the peak frequency, as found in Fig. 2. The local helium (f_{He^+}) and oxygen (f_{O^+}) gyrofrequencies marked by solid dots are the estimated values at the equatorial plane for the magnetic field intensity of Athabasca L shell ($L = 4.6$) calculated from the dipole field model.

Fig. 4b illustrates the wave power at peak frequency. The wave power is plotted for the sample using a threshold value greater than 2.4×10^{-8} (the horizontal dashed line in Fig. 4b) in the unit of $(\text{nT})^2\text{Hz}$. By comparing time-modulated wave activities seen in the dynamic power spectrum in Fig. 2 and the timing of power enhancement in Fig. 4b, this threshold value of wave power is reasonable. Fig. 4c shows the coherence (red dots) and degree of polarization (blue dots). The coherence is distributed in the range of ~ 0.1 – 0.9 , and the degree of polarization is in the range of ~ 0.4 – 0.9 . High-degree of polarization samples in Fig. 4 do not correspond to always high-coherence samples. For example, the samples for the interval of $\sim 15:00$ – $15:30$ UT show a high degree of polarization ($R > 0.8$) while the coherence is low ($\gamma < 0.7$) for that interval. These high-degree of polarization samples are due to a large-amplitude difference between the pulsations in the H and D components, which is confirmed in the dynamic spectra of Fig. 2. The low coherence for the samples indicates that the phase delay of the pulsations between H and D is not constant for the 3-min interval, as noted by Kim et al. (2016b). Thus, we calculate the ellipticity for the high-coherence ($\gamma > 0.7$) samples in Fig. 4d, which are left-handed polarized.

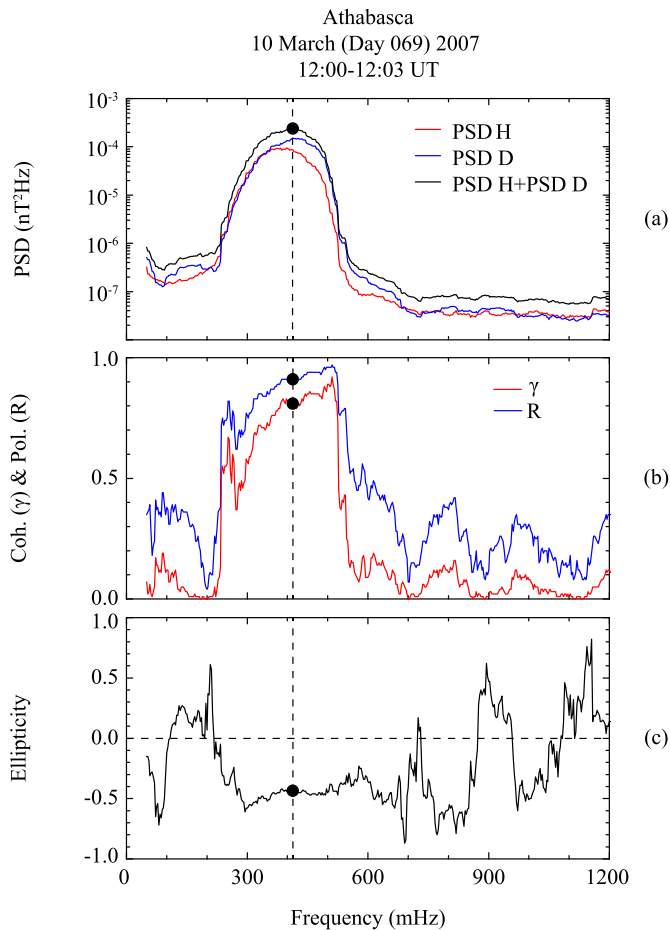


Fig. 3. (a) The power spectral density for the Athabasca *H* and *D* components (PSD *H* and PSD *D*) and total horizontal power density defined to be PSD *H* + PSD *D*. (b) The coherence (γ) and degree of the polarization (*R*) computed for the Athabasca *H* and *D* data. (c) The ellipticity.

4. Statistical analysis

We automated the wave sample selection procedure described above for a statistical analysis and identified 10,494 wave samples in 3-min data segments from the Athabasca data. We also applied the automated procedure to identify EMIC Pc1-Pc2 waves at GOES 11 and identified 12,113 samples. To examine the local time dependence of Pc1-Pc2 wave frequency at geosynchronous orbit and subauroral latitude on the ground, we plotted the peak frequencies of all samples, shown by small gray dots, as a function of GOES 11 (G11LT) and Athabasca local time (ATHLT)-universal time (UT) in Fig. 5. The blue dots indicate the median value within each 1-h local time bin, and the vertical bars connect the upper and lower quartiles.

At GOES 11 two distinct branches in the frequency distribution are apparent for the intervals of 00:00–06:00 UT (LT = 15.0–21.0) and 21:00–24:00 UT (LT = 12.0–15.0). The upper (lower) branch corresponds to the H-band (He-band) EMIC wave. The median values and upper-lower quartiles are plotted in the lower branch for the intervals, indicating that the majority of samples were detected in the He-band. The median values smoothly decrease from ~250 mHz to ~180 mHz for the interval 00:00–08:00 UT (LT = 15.0–23.0) and then suddenly go up to ~440–570 mHz in the upper branch (i.e., H-band) for the interval of 09:00–15:00 UT (LT = 24.0–6.0). The median values for the interval of 16:00–24:00 UT (LT = 7.0–15.0) do not depend much on the UT (or LT), staying at ~270–280 mHz.

Although there is considerable scatter of the frequency samples, the median values at Athabasca gradually increase from ~370 mHz at 00:00

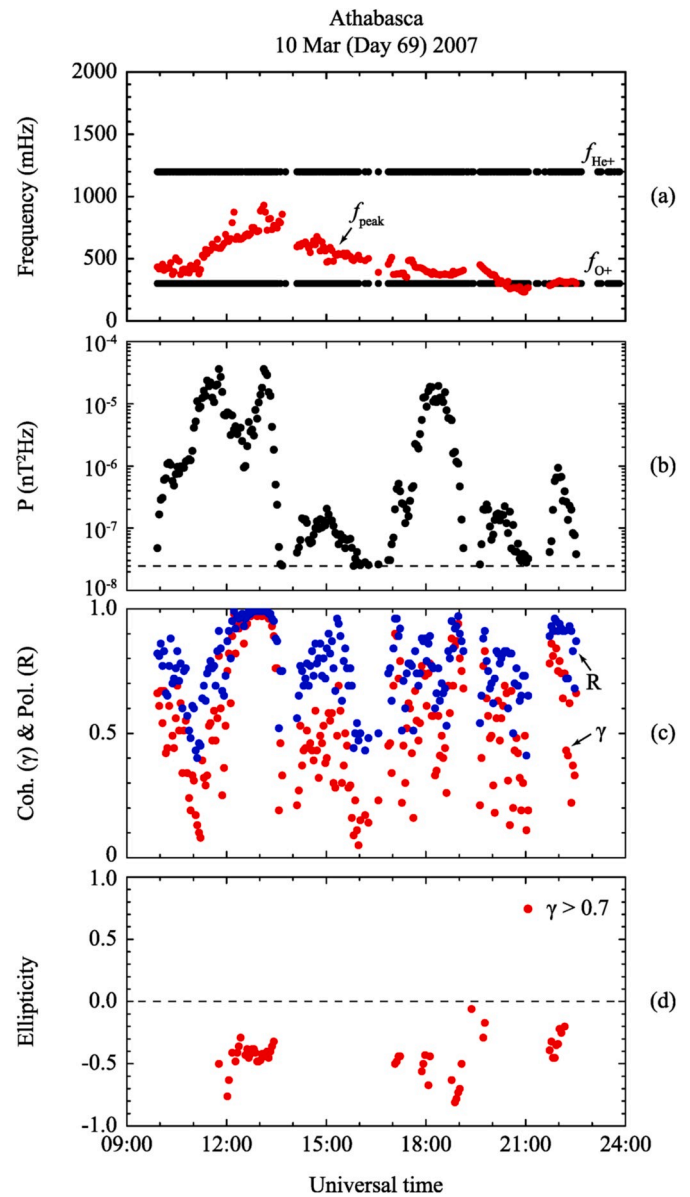


Fig. 4. (a) Peak frequency (f_{peak}) of wave samples (red dots) and the local helium (f_{He^+}) and oxygen (f_{O^+}) gyrofrequencies at the Athabasca L shell (black dots). (b) The wave power at peak frequency. (c) The coherence (red dots) and degree of polarization (blue dots). (d) The ellipticity for high-coherence ($\gamma > 0.7$) samples. (For interpretation of the references to colour in this figure legend, the reader is referred to the Web version of this article.)

UT (LT = 16.5) to ~720 mHz at 10:00 UT (LT = 2.5) and then decrease to ~390 mHz at 24:00 UT without sudden transitions. That is, the median values show a clear tendency with frequencies higher in the postmidnight-to-dawn sector (LT ~ 0–6) and decrease toward the late afternoon sector. This local time dependence of Pc1-Pc2 wave frequencies is not new. Kim et al. (2016a) reported very similar longitudinal frequency variation of a band-limited spectral enhancement, lasting more than 20 h, in the Pc1-Pc2 frequency band and showed that strong spectral enhancements of Pc1-Pc2 waves are in the frequency band between the helium (f_{He^+}) and oxygen (f_{O^+}) gyrofrequencies at the equatorial plasmopause location, which is estimated from localized proton enhancement events observed at low-altitude polar-orbiting satellites. In order to examine how the frequencies of wave samples at Athabasca are distributed with respect to f_{He^+} and f_{O^+} , the equatorial gyrofrequencies, f_{He^+} (upper red solid curve) and f_{O^+} (lower red solid

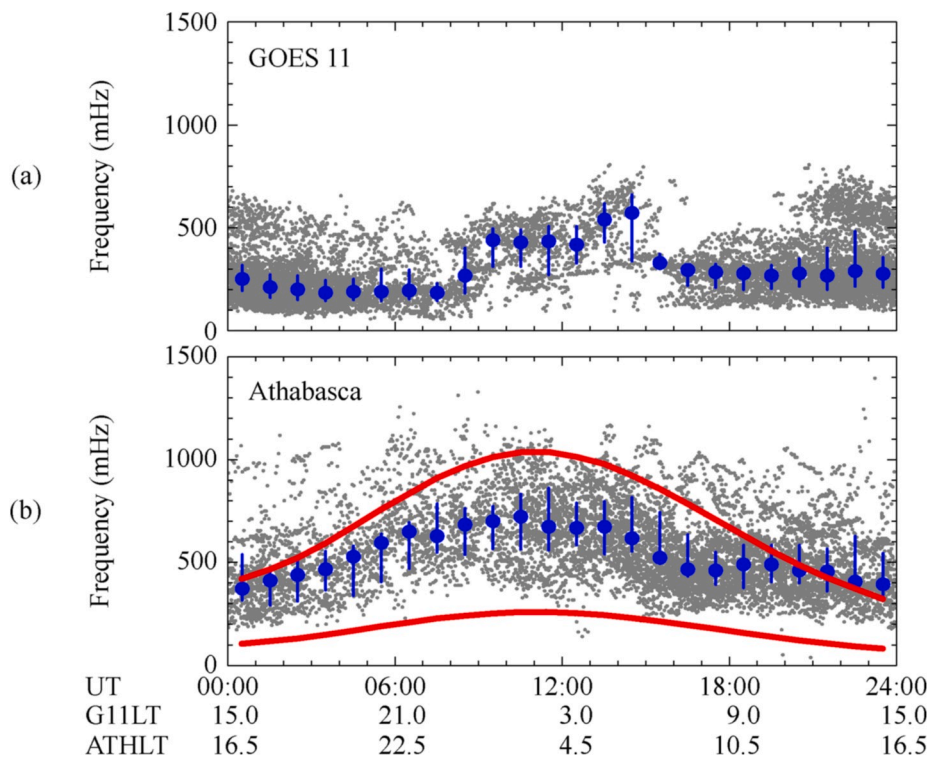


Fig. 5. Peak frequencies of all samples (gray dots) as a function of local time (LT) and universal time (UT) at (a) GOES 11 and (b) Athabasca. The blue dots indicate the median value within each 1-h local time bin, and the vertical bars connect the upper and lower quartiles. The upper and lower solid curves in Fig. 5b indicate f_{He^+} and f_{O^+} , respectively, at the equatorial plasmapause location estimated from localized proton enhancement events (Kim et al., 2016a). (For interpretation of the references to colour in this figure legend, the reader is referred to the Web version of this article.)

curve) estimated by Kim et al. (2016a), are plotted in Fig. 5b. It is found that most of wave samples are located between f_{He^+} and f_{O^+} . This indicates that the Pc1-Pc2 wave power observed at Athabasca ($L \sim 4.6$) is mainly enhanced in the helium band and that the local time variation of the wave frequency is attributed to the asymmetric plasmapause location along the local time (i.e., larger plasmapause distance in the dusk sector and smaller distance in the dawn sector) (e.g., Chappell et al., 1971; Moldwin et al., 2002; Kwon et al., 2015).

Out of 10,494 wave samples at Athabasca, we found that 972 samples (~9%) were simultaneously identified at GOES 11. Fig. 6 shows

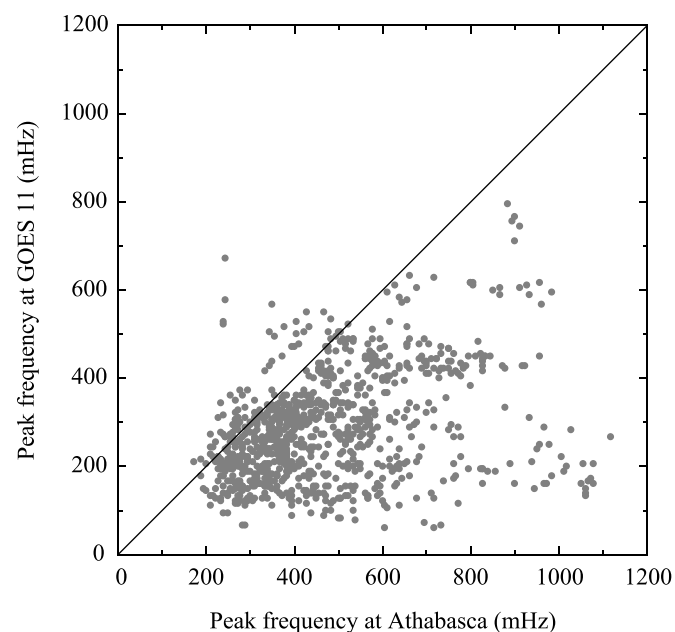


Fig. 6. Frequencies of Pc1-Pc2 wave samples identified simultaneously at GOES 11 and Athabasca.

peak frequencies of the 972 samples identified simultaneously at GOES 11 and Athabasca. As expected in Fig. 5, the majority of the samples at Athabasca have frequencies higher than at GOES 11. This gives a low association of Pc1-Pc2 waves at Athabasca with the waves at GOES 11. Since characteristics of EMIC Pc1-Pc2 waves at geosynchronous orbit have been comprehensively studied by previous studies (e.g., Clausen et al., 2011; Park et al., 2016; Kim et al., 2016b), we mainly focus on the Pc1-Pc2 waves at subauroral latitude on the ground in this study.

We have examined whether there is a K_p dependence of peak frequencies by plotting f_{peak} and $f_{\text{peak}}/f_{\text{H}^+}$ as a function of LT for all K_p conditions, moderate and disturbed conditions ($K_p \geq 2$), and quiet conditions ($K_p \leq 1$), respectively, for the Athabasca samples in Fig. 7. Here f_{H^+} is the equatorial proton gyrofrequency at $L = 4.6$, which is calculated using the background magnetic field intensity at $L = 4.6$ estimated by using the dipole field model. The large blue dots are medians in 1-h LT bins, and the vertical bars connect the upper and lower quartiles in each LT bin. The horizontal dashed lines in Fig. 7d–f indicate the estimated equatorial helium and oxygen gyrofrequencies at $L = 4.6$.

f_{peak} is mostly in the frequency range between f_{He^+} and f_{O^+} even though the data points are scattered. The plot of $f_{\text{peak}}/f_{\text{H}^+}$ versus LT for $K_p \geq 2$ is similar to that for $K_p \leq 1$ in terms of the LT dependence of wave frequency and the data spread with LT. That is, the median value of $f_{\text{peak}}/f_{\text{H}^+}$ monotonically decreases from postmidnight to morning, the LT profile of the median value is nearly flat in the 0800–1800 LT sector, and the data spread is larger in the postmidnight LT bins than that in the afternoon sector. Under quiet geomagnetic conditions ($K_p \leq 1$), the number of samples considerably decreases in the dusk sector, and the wave samples were not detected in a local time sector of LT = 20–22. We show later in Fig. 9 the occurrence rate of wave samples for LT under different geomagnetic conditions.

In order to examine the dependence of f_{peak} on geomagnetic activity, the median values for $K_p \leq 1$ (blue dots) and $K_p \geq 2$ (red dots) are plotted as a function of LT in Fig. 8. From comparison of the median values, we have noted that the median frequencies in the local time sector of postmidnight to prenoon are larger for $K_p \geq 2$ than for $K_p \leq 1$. By contrast, the median f_{peak} lacks a dependence of K_p in the postnoon-

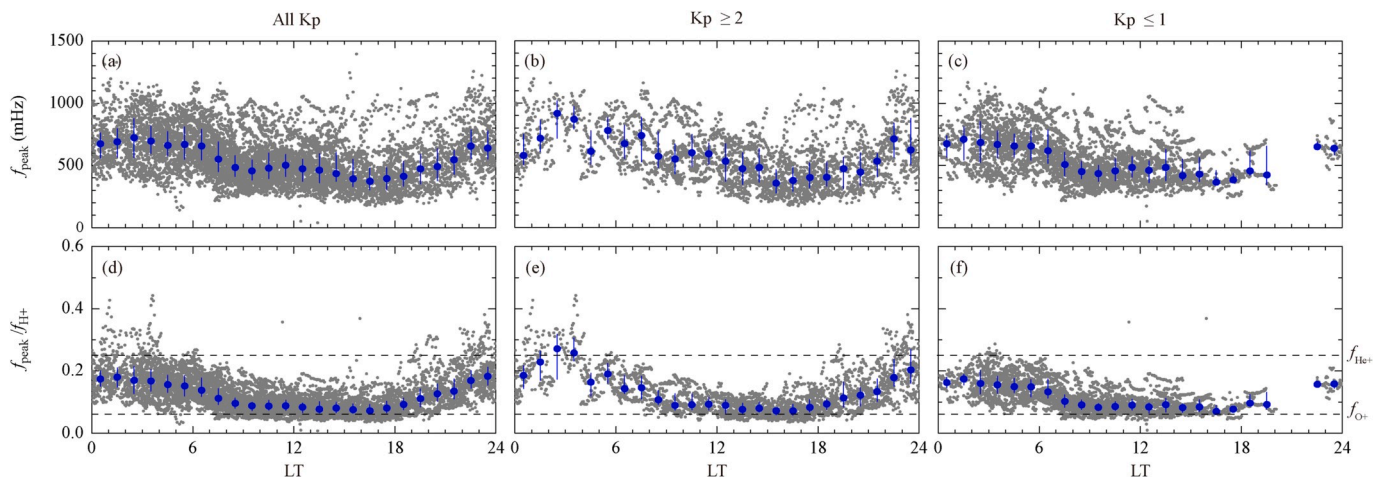


Fig. 7. (a)–(c) f_{peak} and (d)–(f) $f_{\text{peak}}/f_{\text{H}^+}$ as a function of LT for all K_p conditions, moderate and disturbed conditions ($K_p \geq 2$), and quiet conditions ($K_p \leq 1$). The large blue dots are medians in 1-h LT bins, and the vertical bars connect the upper and lower quartiles in each LT bin. The horizontal dashed lines in Fig. 7d–f indicate the estimated equatorial helium and oxygen gyrofrequencies at $L = 4.6$. (For interpretation of the references to colour in this figure legend, the reader is referred to the Web version of this article.)

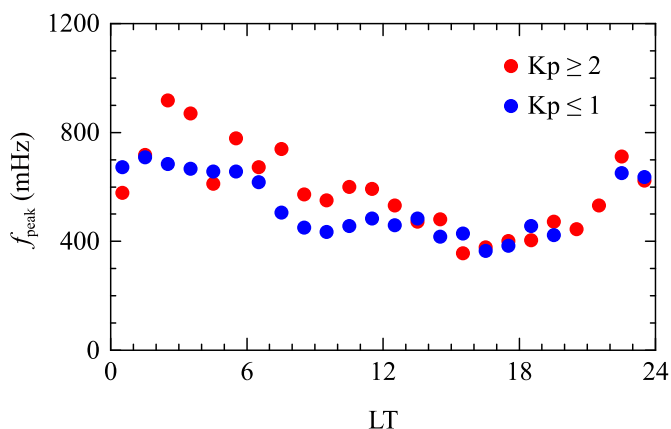


Fig. 8. The median values for $K_p \leq 1$ (blue dots) and $K_p \geq 2$ (red dots) plotted as a function of LT. (For interpretation of the references to colour in this figure legend, the reader is referred to the Web version of this article.)

to-midnight sector.

Fig. 9a shows the distribution of Athabasca observation time versus LT under different geomagnetic conditions for a 2-year period from January 2007 to December 2008. For that time period, the local time occurrence distributions of the wave samples under different geomagnetic conditions are compared in Fig. 9b. As mentioned above, each wave sample was identified for a 3-min interval. Thus, the number of samples is equal to the number of 3-min segments. The occurrence rates, defined to be the sample observation time divided by the total observation time for each 1-h local time bin, for the three different geomagnetic conditions are plotted in Fig. 9c–e. Comparing Fig. 9d and e, we found that the local time dependence of the wave occurrence rate for $K_p \geq 2$ is quite different from that for $K_p \leq 1$. That is, the occurrence rate under quiet geomagnetic conditions has a peak in the prenoon sector at the 0900–1100 LT. This result is consistent with the observations at geosynchronous orbit (Park et al., 2016; Kim et al., 2016b). Under moderate and disturbed geomagnetic conditions, however, the occurrence rate is high in the postnoon sector of 1300–1900 LT, which is a favored local time region of EMIC wave generation (e.g., Anderson et al., 1992b; Clausen et al., 2011).

Fig. 10a shows a scatterplot of ellipticity versus LT for the high-coherence ($\gamma > 0.7$) samples, and Fig. 10b shows the occurrence distribution of the ellipticity. The high-coherence samples are about 42%

(4411 out of 10494) of the total wave samples. This rate is higher than at geosynchronous orbit by a factor of ~ 4 (Kim et al., 2016b). It is clear that the distribution of the ellipticity along local time is considerably scattered within the -0.9 to 0.9 range. Although the distribution is skewed toward negative values (left-hand polarization) with a peak occurrence between -0.4 and -0.2 , $\sim 40\%$ (1766 out of 4411) of the high-coherence samples were observed with the positive ellipticity (right-hand polarization). This indicates that the Pc1-Pc2 waves observed at Athabasca were composed of a mixture of left-handed, right-handed, and linear polarized waves.

5. Discussion

This study is motivated by a recent case study of long-lasting (>20 h) EMIC Pc1-Pc2 waves observed at Athabasca ($L \sim 4.6$) on April 5, 2007 (Kim et al., 2016a). The Pc1-Pc2 waves were localized in the inner magnetosphere inside geosynchronous orbit, and their frequencies changed with LT (i.e., the minimum frequency near dusk and the maximum frequency near dawn) in the He-band between the equatorial helium and oxygen gyrofrequencies at the estimated plasmopause. During the wave activities, localized proton enhancement (LPE) events were detected at low-altitude polar-orbiting spacecraft. The equatorial radial distance (L) of the magnetic shell corresponding to the location of the LPE event shows a systematic variation of LT. That is, a minimum of L is near dawn, and a maximum of L is near the afternoon. Consequently, LPE events were detected at lower (higher) L for the interval of higher (lower) frequency waves (see Fig. 5 in Kim et al., 2016a). The authors suggested that the LPE events are associated with the result of wave-particle interactions with EMIC waves generated near the asymmetric plasmopause location along the local time.

Sakaguchi et al. (2007, 2008) reported simultaneous appearance of isolated proton auroras and Pc1 geomagnetic pulsations at the Athabasca station of subauroral latitudes. The auroral arcs appeared at lower (higher) latitudes when Pc1 waves were detected at higher (lower) frequencies. The authors found that the isolated aurora arcs are associated with the localized enhancement of energetic (~ 30 – 80 keV) ions precipitating from a region connected near $L = 4$ and suggested that the coincident precipitation with Pc1 wave occurrence at subauroral latitudes is due to wave-particle interactions with EMIC waves generated near the plasmopause. They also reported that the Pc1 waves are in the frequency range of the He-band. From the previous studies showing a close relationship between localized energetic proton enhancements and Pc1-Pc2 wave occurrences at subauroral latitudes (Sakaguchi et al.,

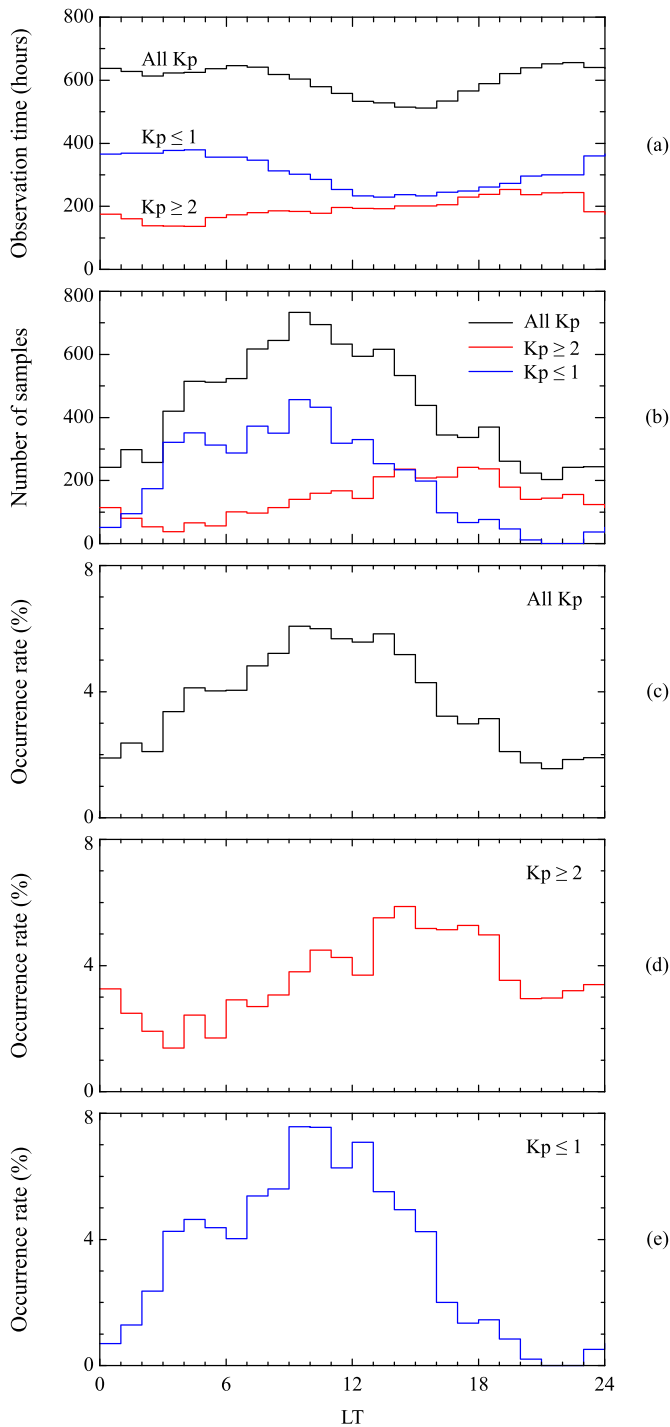


Fig. 9. (a) The distribution of Athabasca observation time versus LT under different geomagnetic conditions for a 2-year period from January 2007 to December 2008. (b) The local time occurrence distributions of the wave samples under different geomagnetic conditions. (c)–(e) The occurrence rates, defined to be the sample observation time divided by the total observation time for each 1-h local time bin, for the three different geomagnetic conditions.

2007, 2008; Kim et al., 2016a), we suggest that the Pc1-Pc2 waves observed at Athabasca are generated near the plasmopause.

In the present study, we statistically examined whether Pc1-Pc2 waves observed at Athabasca show the characteristics of the long-lasting Pc1-Pc2 waves reported in the case study by Kim et al. (2016a) and confirmed that our statistical results are similar to the wave properties in that case study. The median values of wave frequencies made in

1-hr local time bins clearly exhibit LT dependencies with a maximum near dawn and a minimum near late afternoon, and that the wave samples are mostly detected in the He-band, as shown in Fig. 5. The median values of $f_{\text{peak}}/f_{\text{H}^+}$ monotonically decrease from dawn to late afternoon in the He-band for $Kp \leq 1$ and $Kp \geq 2$ (see Fig. 8). This frequency behavior is similar to that at geosynchronous orbit under steady quiet conditions (Kim et al., 2016b).

Using THEMIS data in the outer magnetosphere, Min et al. (2012) and Kim et al. (2016c) reported that the maximum occurrence rate of H-band EMIC waves is in the outer most region ($L = 10\text{--}12$) of the magnetosphere in the morning sector, and that He-band waves exhibit a peak occurrence rate in the afternoon sector at $L = 8\text{--}10$. These spatial distributions of the H-band and He-band EMIC wave occurrences in the outer magnetosphere ($L > 7$) have been attributed to the asymmetric cold plasma density distribution along the local time, implying that the cold plasma density plays an important role in determining the spectral properties of EMIC waves. Kim et al. (2016c) found that the cold plasma density is much higher for the He-band wave intervals than for the H-band wave intervals by a factor of 10 or more. This indicates that He-band waves are more frequently observed than H-band waves in the inner magnetosphere ($L < 7$) (e.g., Keika et al., 2013; Meredith et al., 2014; Saikin et al., 2015). In the Earth’s magnetosphere, cold plasmaspheric plasmas contain heavy ions (primarily O^+ and He^+). Previous studies reported that the great amplification of EMIC waves occur in the He-band even though a small amount of He^+ ions exist in the magnetosphere (e.g., Young et al., 1981; Kozyra et al., 1984). Thus, He-band wave samples detected at Athabasca are associated with EMIC waves generated in a region of cold and dense plasmas containing heavy ions in the inner magnetosphere.

It has been suggested that a region near the plasmopause is one of the favored regions for the generation of EMIC waves because EMIC wave growth is enhanced by increasing the cold background plasma density (e.g., Kozyra et al., 1984). Fraser et al. (1989) reported that Pc1 waves observed at middle-latitude ground stations are generated near the plasmopause. Since the magnetic L shell of Athabasca ($L \sim 4.6$) is close to the typical location of the plasmopause ($L = \sim 4\text{--}5$), we suggest that the source region of Pc1-Pc2 waves observed at Athabasca is near the plasmopause. The Pc1-Pc2 wave properties observed at Athabasca may be attributed to the background magnetic field intensity and plasma conditions in the vicinity of the plasmopause because EMIC wave frequency is determined by the energy and anisotropy of energetic ions, ion composition of cold and energetic ions, cold plasma density, and background magnetic field intensity (Gomberoff and Neira, 1983; Kozyra et al., 1984; Horne and Thorne, 1994). This is why we have data points of wave frequencies considerably scattered in each local time bin (see Figs. 5 and 7).

Recently, Kwon et al. (2015) reported that the plasmopause has a larger radius at an afternoon-to-dusk sector than at a postmidnight sector under moderate geomagnetic conditions. The median values of the wave frequencies show a systematic change with local times (i.e., higher in 0.5–6.5 LT and lower in 12–18 LT). Thus, we suggest that the local time dependence of Pc1-Pc2 wave frequencies shown in Figs. 5b and 7 is due to the asymmetric plasmopause location along the local time. Fig. 11 shows longitudinal variations of the hourly median values of peak frequencies at Athabasca and the hourly medians of the plasmopause distance L_{pp} under moderate geomagnetic conditions reported by Kwon et al. (2015). The L_{pp} medians show a bulge formed in the dusk sector above $L = 6$. Around this local time sector, the median frequency is lower, and the median frequency in the $\sim 0.0\text{--}7.0$ LT sector is higher when the median L_{pp} is closer to the earth ($L_{\text{pp}} < 5$). It is possible to explain the frequency behavior in terms of the background magnetic field intensity near the longitudinally asymmetric plasmopause. Since Athabasca is located on a magnetic L shell of 4.6, as noted above, the Pc1-Pc2 waves detected in the dawn and dusk sectors are attributed to the waves ducted from lower and higher L shell regions, respectively, in the vicinity of the plasmopause.

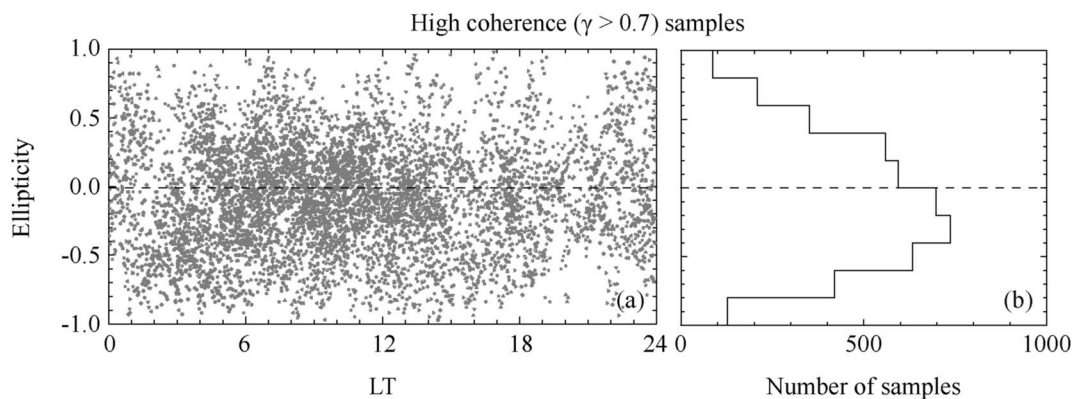


Fig. 10. (a) A scatterplot of ellipticity versus LT for the high-coherence ($\gamma > 0.7$) samples. (b) The occurrence distribution of the ellipticity.

Kwon et al. (2015) also reported that the plasmapause location in the local time sector of 00–12 LT expands under quiet time geomagnetic conditions ($Kp \leq 1$). Since the He-band EMIC wave frequency decreases with increasing cold plasma density (e.g., Kim et al., 2016b), the frequencies lower for $Kp \leq 1$ than for $Kp \geq 2$ in the 00–12 LT sector shown in Fig. 8 may be due to the expansion of the plasmasphere.

We observed that the occurrence rate of Pc1-Pc2 waves at Athabasca is higher in the postnoon sector (13–19 LT) under moderate and disturbed geomagnetic conditions ($Kp \geq 2$). This result is consistent with the local time occurrence distribution of the He-band EMIC waves reported in previous studies (e.g., Anderson et al., 1992b; Clausen et al., 2011; Keika et al., 2013; Meredith et al., 2014; Park et al., 2016). This high-occurrence longitudinal region corresponds to the bulge region of the plasmasphere or plasmaspheric plumes. Many theoretical studies have described that enhanced cold plasmaspheric density increases the growth rate of EMIC waves (e.g., Cornwall et al., 1970; Kozyra et al., 1984). Since energetic ring current and plasma sheet ions, which are considered as the source of EMIC instability and drifting westward, encroach on the cold plasmaspheric plasmas in the dusk sector, the EMIC wave growth can maximize in the bulge and plume regions during moderate and disturbed geomagnetic conditions.

Unlike the local time occurrence distribution of Pc1-Pc2 waves under moderate and disturbed geomagnetic conditions, the occurrence rate is higher in the prenoon sector with a peak near 0900–1100 LT, which is consistent with geosynchronous observations (Park et al., 2016; Kim

et al., 2016b) under quiet geomagnetic conditions ($Kp \leq 1$). Hyun et al. (2014) and Park et al. (2016) reported that EMIC waves can be generated by even small solar wind dynamic pressure enhancements under quiet geomagnetic conditions at geosynchronous orbit. Although the magnetic shell of Athabasca is inside the geosynchronous orbit, we suggest that the high occurrence of the Pc1-Pc2 waves near noon in the inner magnetosphere is due to dayside magnetospheric perturbations caused by small solar wind dynamic pressure changes.

In the scatter plot of Fig. 10, the ellipticities for high-coherence ($\gamma > 0.7$) wave samples are distributed between -0.9 and 0.9 without local time dependence even though the distribution is slightly skewed toward negative values. That is, the Pc1-Pc2 waves at Athabasca exhibit the coexistence of left-handed, right-handed, and linear polarized waves. This is significantly different from the geosynchronous observations reported by Kim et al. (2016b). They observed that ellipticities of high-coherence ($\gamma > 0.7$) He-band EMIC waves at geosynchronous orbit over 0600–1800 magnetic local time are mainly distributed below zero, and the median values are distributed in the range of -0.5 to -0.2 . This indicates that geosynchronous He-band waves are left-hand polarized. The difference between polarizations of signals detected in space and on the ground is not surprising because the polarization of ground signals varies as a function of radial distance from a source region (Greifinger, 1972; Fujita and Tamao, 1988). Thus, we suggest that the ellipticity distribution, spreading over a wide range between -0.9 and 0.9 , of the Pc1-Pc2 waves at Athabasca is due to the fact that the wave source in the magnetosphere is not a localized point, but a longitudinally and radially extended region near the equatorial plasmapause.

6. Conclusion

Using the induction magnetometer data obtained at a subauroral station Athabasca ($L \sim 4.6$), we have statistically investigated subauroral latitude Pc1-Pc2 waves. We clearly showed that the frequencies of Pc1-Pc2 waves are mostly in the He-band and that their median frequencies made in 1-hr local time bins depend on the local time. That is, the frequency is higher in the postmidnight sector, and the frequency is lower late afternoon. This frequency behavior showing longitudinal variation of Pc1-Pc2 wave frequency may be due to the asymmetric plasmapause location along the local time. Additionally, we have examined the properties of the Pc1-Pc2 waves under different geomagnetic conditions and found that the median wave frequencies in the 00–12 LT sector are lower for $Kp \leq 1$ than for $Kp \geq 2$. This observation can also be explained by the radial distance of the plasmapause expanded under quiet conditions. Based on our study, we suggest that subauroral latitude Pc1-Pc2 waves are associated with EMIC waves generated near the plasmapause. In future studies, we will use the data from Van Allen Probes and ERG mission to determine the degree that the sources near the plasmapause contribute to EMIC wave generation in the

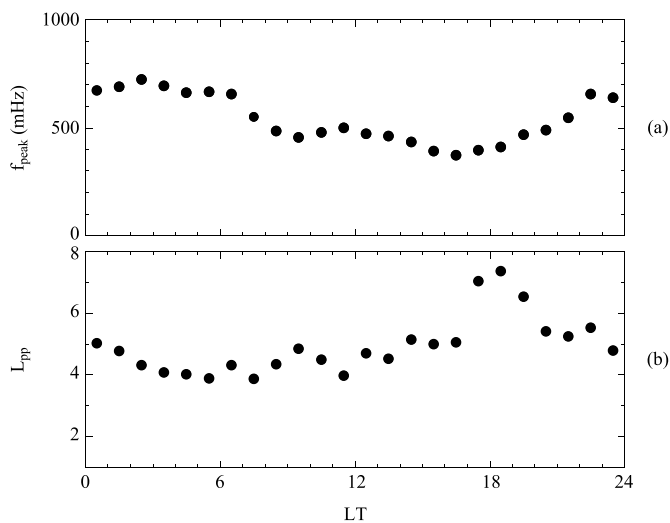


Fig. 11. Local time dependence of (a) the hourly median values of peak frequencies at Athabasca station and (b) the hourly medians of the plasmapause distance L_{pp} (Kwon et al., 2015).

inner magnetosphere.

Acknowledgments

The K_p values were obtained from the World Data Center C2 (WDC-C2) for Geomagnetism, Kyoto University (<http://wdc.kugi.kyoto-u.ac.jp>). The observation at ATH has been supported by JSPS KAKENHI (20244080, 23403009, 25247080, 15H05815, and 16H06286). This work was supported by BK21+ through the National Research Foundation (NRF) funded by the Ministry of Education of Korea. The work of K.-H. Kim was supported by the Basic Science Research Program through NRF funded by NRF-2019R1F1A1055444 and also supported by project PE20100 of the Korea Polar Research Institute.

References

- Anderson, B.J., Erlanson, R.E., Zanetti, L.J., 1992a. A statistical study of Pc 1-2 magnetic pulsations in the equatorial magnetosphere: 1. Equatorial occurrence distributions. *J. Geophys. Res.* 97 (A3), 3075–3088. <https://doi.org/10.1029/91JA02706>.
- Anderson, B.J., Erlanson, R.E., Zanetti, L.J., 1992b. A statistical study of Pc 1-2 magnetic pulsations in the equatorial magnetosphere, 2. Wave properties. *J. Geophys. Res.* 97 (A3), 3089–3101. <https://doi.org/10.1029/91JA02697>.
- Bendat, J.S., Piersol, A.G., 2010. *Random Data: Analysis and Measurement Procedures*. John Wiley, New York.
- Bortnik, J., Cutler, J.W., Dunson, C., Bleier, T.E., McPherron, R.L., 2008. Characteristics of low-latitude Pc1 pulsations during geomagnetic storms. *J. Geophys. Res.* 113, A04201. <https://doi.org/10.1029/2007JA012867>.
- Chappell, C.R., Harris, K.K., Sharp, G.W., 1971. The dayside of the plasmasphere. *J. Geophys. Res.* 76, 7632–7647. <https://doi.org/10.1029/JA076i031p07632>.
- Clausen, L.B.N., Baker, J.B.H., Ruohoniemi, J.M., Singer, H.J., 2011. EMIC waves observed at geosynchronous orbit during solar minimum: statistics and excitation. *J. Geophys. Res.* 116, A10205. <https://doi.org/10.1029/2011JA016823>.
- Cornwall, J.M., Coroniti, F.V., Thorne, R.M., 1970. Turbulent loss of ring current protons. *J. Geophys. Res.* 75 (25), 4699–4709. <https://doi.org/10.1029/JA075i025p04699>.
- Cornwall, J.M., 1965. Cyclotron instabilities and electromagnetic emission in the ultralow frequency and very low frequency ranges. *J. Geophys. Res.* 70 (1), 61–69. <https://doi.org/10.1029/JZ070i001p00061>.
- Engebretson, M.J., Peterson, W.K., Posch, J.L., Klatt, M.R., Anderson, B.J., Russell, C.T., Fukushima, H., 2002. Observations of two types of Pc 1-2 pulsations in the outer dayside magnetosphere. *J. Geophys. Res.* 107 (A12), 1451. <https://doi.org/10.1029/2001JA000198>.
- Engebretson, M.J., Posch, J.L., Wygant, J.R., Kletzing, C.A., Lessard, M.R., Huang, C.-L., Shiokawa, K., 2015. Van Allen probes, NOAA, GOES, and ground observations of an intense EMIC wave event extending over 12 h in magnetic local time. *J. Geophys. Res.: Space Physics* 120, 5465–5488. <https://doi.org/10.1002/2015JA021227>.
- Erlanson, R.E., Ukhorskiy, A.J., 2001. Observations of electromagnetic ion cyclotron waves during geomagnetic storms: wave occurrence and pitch angle scattering. *J. Geophys. Res.* 106 (A3), 3883–3895. <https://doi.org/10.1029/2000JA000083>.
- Fowler, R.A., Kotick, B.J., Elliott, R.D., 1967. Polarization analysis of natural and artificially induced geomagnetic micropulsations. *J. Geophys. Res.* 72 (11), 2871–2883. <https://doi.org/10.1029/JZ072i011p02871>.
- Fraser, B.J., Kemp, W.J., Webster, D.J., 1989. Ground-satellite study of a Pc1 ion cyclotron wave event. *J. Geophys. Res.* 94 (A9) <https://doi.org/10.1029/JA094iA09p11855>, 11,855–11,863.
- Fraser, B.J., Nguyen, T.S., 2001. Is the plasmapause a preferred source region of electromagnetic ion cyclotron waves in the magnetosphere? *J. Atmos. Sol. Terr. Phys.* 63 (11), 1225–1247. [https://doi.org/10.1016/S1364-6826\(00\)00225-X](https://doi.org/10.1016/S1364-6826(00)00225-X).
- Fujita, S., Tamao, T., 1988. Duct propagation of hydromagnetic waves in the upper ionosphere: 1. Electromagnetic field disturbances in high latitudes associated with localized incident of a shear Alfvén wave. *J. Geophys. Res.* 93 (A12) <https://doi.org/10.1029/JA093iA12p14665>, 14,665–14,673.
- Gomberoff, L., Neira, R., 1983. Convective growth rate of ion cyclotron waves in a $H^+ - He^+$ and $H^+ - He^+ - O^+$ plasma. *J. Geophys. Res.* 88 (A3), 2170–2174. <https://doi.org/10.1029/JA088iA03p02170>.
- Greifinger, P., 1972. Micropulsations from a finite source. *J. Geophys. Res.* 77 (13), 2392–2396. <https://doi.org/10.1029/JA077i013p02392>.
- Halford, A.J., Fraser, B.J., Morley, S.K., 2015. EMIC waves and plasmaspheric and plume density: CRRES results. *J. Geophys. Res.: Space Physics* 120, 1974–1992. <https://doi.org/10.1002/2014JA020338>.
- Horne, R.B., Thorne, R.M., 1994. Convective instabilities of electromagnetic ion cyclotron waves in the outer magnetosphere. *J. Geophys. Res.* 99 (A9) <https://doi.org/10.1029/94JA01259>, 17,259–17,273.
- Hyun, K., Kim, K.-H., Lee, E., Kwon, H.-J., Lee, D.-H., Jin, H., 2014. Loss of geosynchronous relativistic electrons by EMIC wave scattering under quiet geomagnetic conditions. *J. Geophys. Res.: Space Physics* 119, 8357–8371. <https://doi.org/10.1002/2014JA020234>.
- Ishida, J., Kokubun, S., McPherron, R.L., 1987. Substorm effects on spectral structures of Pc 1 waves at synchronous orbit. *J. Geophys. Res.* 92 (A1), 143–158. <https://doi.org/10.1029/JA092iA01p00143>.
- Jordanova, V.K., Albert, J., Miyoshi, Y., 2008. Relativistic electron precipitation by EMIC waves from self-consistent global simulations. *J. Geophys. Res.* 113, A00A10. <https://doi.org/10.1029/2008JA013239>.
- Keika, K., Takahashi, K., Ukhorskiy, A.Y., Miyoshi, Y., 2013. Global characteristics of electromagnetic ion cyclotron waves: occurrence rate and its storm dependence. *J. Geophys. Res.: Space Physics* 118, 4135–4150. <https://doi.org/10.1002/jgra.50385>.
- Kennel, C.F., Petschek, H.E., 1966. Limit on stably trapped particle fluxes. *J. Geophys. Res.* 71 (1), 1–28. <https://doi.org/10.1029/JZ071i001p00001>.
- Kim, G.-J., Kim, K.-H., Lee, D.-H., Kwon, H.-J., Park, J.-S., 2016c. Occurrence of EMIC waves and plasmaspheric plasmas derived from THEMIS observations in the outer magnetosphere: Revisit. *J. Geophys. Res.: Space Physics* 121, 9443–9458. <https://doi.org/10.1002/2016JA023108>.
- Kim, K.-H., Park, J.-S., Omura, Y., Shiokawa, K., Lee, D.-H., Kim, G.-J., Kwon, H.-J., 2016b. Spectral characteristics of steady quiet-time EMIC waves observed at geosynchronous orbit. *J. Geophys. Res.: Space Physics* 121, 8640–8660. <https://doi.org/10.1002/2016JA022957>.
- Kim, K.-H., Shiokawa, K., Mann, I.R., Park, J.-S., Kwon, H.-J., Hyun, K., Connors, M., 2016a. Longitudinal frequency variation of long-lasting EMIC Pc1-Pc2 waves localized in the inner magnetosphere. *Geophys. Res. Lett.* 43, 1039–1046. <https://doi.org/10.1002/2015GL067536>.
- Kim, K.-H., Omura, Y., Jin, H., Hwang, J., 2017. A case study of EMIC waves associated with sudden geosynchronous magnetic field changes. *J. Geophys. Res.: Space Physics* 122, 3322–3341. <https://doi.org/10.1002/2016JA023391>.
- Kozyra, J.U., Cravens, T.E., Nagy, A.F., Fongheim, E.G., Ong, R.S.B., 1984. Effects of energetic heavy ions on electromagnetic ion cyclotron wave generation in the plasmapause region. *J. Geophys. Res.* 89 (A4), 2217–2233. <https://doi.org/10.1029/JA089iA04p02217>.
- Kwon, H.-J., Kim, K.-H., Jee, G., Park, J.-S., Jin, H., Nishimura, Y., 2015. Plasmapause location under quiet geomagnetic conditions ($K_p \leq 1$): THEMIS observations. *Geophys. Res. Lett.* 42, 7303–7310. <https://doi.org/10.1002/2015GL066090>.
- Mann, I.R., Usanova, M.E., Murphy, K., Robertson, M.T., Milling, D.K., Kale, A., Raita, T., 2014. Spatial localization and ducting of EMIC waves: Van Allen Probes and ground-based observations. *Geophys. Res. Lett.* 41, 785–792. <https://doi.org/10.1002/2013GL058581>.
- Mauk, B.H., McIlwain, C.E., McPherron, R.L., 1981. Helium cyclotron resonance within the Earth's magnetosphere. *Geophys. Res. Lett.* 8, 103–106. <https://doi.org/10.1029/GL008i001p0103>.
- Meredith, N.P., Horne, R.B., Kersten, T., Fraser, B.J., Grew, R.S., 2014. Global morphology and spectral properties of EMIC waves derived from CRRES observations. *J. Geophys. Res.: Space Physics* 119, 5328–5342. <https://doi.org/10.1002/2014JA020064>.
- Min, K., Lee, J., Keika, K., Li, W., 2012. Global distribution of EMIC waves derived from THEMIS observations. *J. Geophys. Res.: Space Physics* 117, A05219. <https://doi.org/10.1029/2012JA017515>.
- Moldwin, M.B., Downward, L., Rassoul, H.K., Amin, R., Anderson, R.R., 2002. A new model of the location of the plasmapause: CRRES results. *J. Geophys. Res.* 107 (A11), 1339. <https://doi.org/10.1029/2001JA009211>.
- Nomura, R., Shiokawa, K., Pilipenko, V., Shevtsov, B., 2011. Frequency-dependent polarization characteristics of Pc1 geomagnetic pulsations observed by multipoint ground stations at low latitudes. *J. Geophys. Res.* 116, A01204. <https://doi.org/10.1029/2010JA015684>.
- Olson, J.V., Lee, C.C., 1983. Pc1 wave generation by sudden impulses. *Planet. Space Sci.* 31 (3), 295–302. [https://doi.org/10.1016/0032-0633\(83\)90079-X](https://doi.org/10.1016/0032-0633(83)90079-X).
- Park, J.-S., Kim, K.-H., Shiokawa, K., Lee, D.-H., Lee, E., Kwon, H.-J., Jee, G., 2016. EMIC waves observed at geosynchronous orbit under quiet geomagnetic conditions ($K_p \leq 1$). *J. Geophys. Res.: Space Physics* 121, 1377–1390. <https://doi.org/10.1002/2015JA021968>.
- Roux, A., Perraut, S., Rauch, J.L., de Villardry, C., Kremser, G., Korth, A., Young, D.T., 1982. Wave-particle interactions near Ω_{He^+} observed on board GEOS 1 and 2: 2. Generation of ion cyclotron waves and heating of He^+ ions. *J. Geophys. Res.* 87 (A10), 8174–8190. <https://doi.org/10.1029/JA087iA10p08174>.
- Sakaguchi, K., Shiokawa, K., Ieda, A., Miyoshi, Y., Otsuka, Y., Ogawa, T., Rich, F.J., 2007. Simultaneous ground and satellite observations of an isolated proton arc at subauroral latitudes. *J. Geophys. Res.* 112, A04202. <https://doi.org/10.1029/2006JA012135>.
- Sakaguchi, K., Shiokawa, K., Miyoshi, Y., Otsuka, Y., Ogawa, T., Asamura, K., Connors, M., 2008. Simultaneous appearance of isolated auroral arcs and Pc 1 geomagnetic pulsations at subauroral latitudes. *J. Geophys. Res.* 113, A05201. <https://doi.org/10.1029/2007JA012888>.
- Saikin, A.A., Zhang, J.-C., Allen, R.C., Smith, C.W., Kistler, L.M., Spence, H.E., Jordanova, V.K., 2015. The occurrence and wave properties of H^+ , He^+ , and O^+ band EMIC waves observed by the Van Allen Probes. *J. Geophys. Res.: Space Physics* 120, 7477–7492. <https://doi.org/10.1002/2015JA021358>.
- Shepherd, S.G., 2014. Altitude-adjusted corrected geomagnetic coordinates: definition and functional approximations. *J. Geophys. Res.* 119, 7501–7521. <https://doi.org/10.1002/2014JA020264>.
- Shiokawa, K., Nomura, R., Sakaguchi, K., Otsuka, Y., Hamaguchi, Y., Satoh, M., Connors, M., 2010. The STEL induction magnetometer network for observation of high-frequency geomagnetic pulsations. *Earth Planets Space* 62, 517–524. <https://doi.org/10.5047/eps.2010.05.003>.
- Singer, H., Matheson, L., Grubb, R., Newman, A., Bouwer, D., 1996. Monitoring space weather with the GOES magnetometers. In: Washwell, E.R. (Ed.), *Society of Photo-Optical Instrumentation Engineers (SPIE) Conference Series*, vol. 2812. Soc. of Photo-Opt. Instrum. Eng., Bellingham, Wash, pp. 299–308. <https://doi.org/10.1117/12.254077>.

- Tetrick, S.S., Engebretson, M.J., Posch, J.L., Olson, C.N., Smith, C.W., Denton, R.E., Fennell, J.F., 2017. Location of intense electromagnetic ion cyclotron (EMIC) wave events relative to the plasmopause: Van Allen Probes observations. *J. Geophys. Res.: Space Physics* 122, 4064–4088. <https://doi.org/10.1002/2016JA023392>.
- Tsyganenko, N.A., 1989. A magnetospheric magnetic field model with a warped tail current sheet. *Planet. Space Sci.* 37 (1), 5–20. [https://doi.org/10.1016/00320633\(89\)90066-4](https://doi.org/10.1016/00320633(89)90066-4).
- Usanova, M.E., Mann, I.R., Bortnik, J., Shao, L., Angelopoulos, V., 2012. THEMIS observations of electromagnetic ion cyclotron wave occurrence: dependence on AE, SYMH, and solar wind dynamic pressure. *J. Geophys. Res.* 117, A10218. <https://doi.org/10.1029/2012JA018049>.
- Usanova, M.E., Mann, I.R., Rae, I.J., Kale, Z.C., Angelopoulos, V., Bonnell, J.W., Singer, H.J., 2008. Multipoint observations of magnetospheric compression-related EMIC Pc1 waves by THEMIS and CARISMA. *Geophys. Res. Lett.* 35, L17S25. <https://doi.org/10.1029/2008GL034458>.
- Young, D.T., Perraut, S., Roux, A., de Villedary, C., Gendrin, R., Korth, A., Jones, D., 1981. Wave-particle interactions near Ω_{He^+} observed on GEOS 1 and 2 1. Propagation of ion cyclotron waves in He⁺-rich plasma. *J. Geophys. Res.* 86 (A8), 6755–6772. <https://doi.org/10.1029/JA086iA08p06755>.